Received <day> <Month>, <year>; | Revised <day> <Month>, <year>; | Accepted <day> <Month>, <year>

DOI: xxx/xxxx

ARTICLE TYPE

Kinetics and Thermodynamics of CO Oxidation by $(TiO_2)_6$

Navjot Kaur[1,2] | Neetu Goel*[1] | Michael Springborg*[3,4] | Mohammad Molayem[3]

[1] Guru Gobind Singh College For Women Sector 26, Chandigarh, 160019, India
[2]Theoretical and Computational Chemistry Group, Department of Chemistry, Centre of Advanced Studies in Chemistry, Panjab University, Chandigarh, 160014,India
[3]Physical and Theoretical Chemistry, University of Saarland, Saarbrücken, 66123, Germany
[4]School of Materials Science and Engineering, Tianjin University, Tianjin, 300072, P.R. China

Correspondence
*Neetu Goel, Theoretical and Computational Chemistry Group, Department of Chemistry, Centre of Advanced Studies in Chemistry, Panjab University, Chandigarh, 160014, India Email: neetugoel@pu.ac.in
*Michael Springborg, Physical and Theoretical Chemistry, University of Saarland, Saarbrücken, 66123, Germany Email: m.springborg@mx.uni-saarland.de

Abstract

Molecular level insights into the mechanism and thermodynamics of CO oxidation by a $(TiO_2)_6$ cluster have been obtained through density functional calculations. Thereby, we have considered as an example, two different structural isomers of $(TiO_2)_6$ with the purpose of understanding the interplay between local structure and activity for the CO oxidation reaction. Active sites in the two isomeric forms were identified on the basis of global and local reactivity descriptors. For the oxidation of CO to CO_2 we considered both sequential and simultaneous adsorption of CO and O_2 on $(TiO_2)_6$ cluster through the ER and LH mechanisms, respectively. Three different pathways were obtained for CO oxidation by $(TiO_2)_6$ cluster, and the mechanistic route of each pathway were identified by locating the transition-state and intermediate structures. The effects of temperature on the rate of the reaction was investigated within the harmonic approximation. The structure-dependent activity of the cluster was rationalized through reactivity descriptors and analysis of the frontier orbitals. Finally, we also considered the effects of a support, i.e., graphene, on the oxidation mechanism.

KEYWORDS:
Catalytic Effects, Metal-Oxide Clusters, Graphene, Temperature effects

1 | INTRODUCTION

The oxidation of carbon monoxide to carbon dioxide holds much importance for the abatement of the environmental pollution. Oxides of various transition metals such as those of iron,[1,2,3] cobalt,[4,5] nickel,[6] and titanium[7,8] have been explored as heterogenous catalysts to facilitate this conversion. Among all the transition metal oxides, titanium oxide has attracted much attention owing to its photocatalytic and hydrophilic properties.[9,10,8,7,11] Several advantages such as high photoactivity, good stability, high corrosion resistance and low price offered by TiO_2 nanoparticles make them attractive heterogeneous catalysts.[12,13,14] It has been demonstrated that TiO_2 plays a decisive role in CO oxidation by metallic clusters anchored on the surface of TiO_2.[15,16,17] Apart from its role as active support, this metal oxide has found applicability in many industrial processes including solar cells, environmental cleanup and photocatalysis.[13,11] In a recent study, TiO_2 supported on graphene has been suggested as a candidate for CO_2 reduction.[18] The present work explores the suitability of this transition metal oxide for CO oxidation.

In order to design an effective catalyst for any reaction, a deep understanding of the underlying chemical processes is needed. This, in turn, is sensitive to the size, composition and morphology of the active material. In particular, CO oxidation is reported to show strong dependence on size and composition of the catalyst as well as that of the support material.[19,20] For instance, Reddy and Khanna have investigated the reactivity of a bare Fe_2O_3 cluster for the oxidation of CO to CO_2 through composition

changes between Fe_2O_2 and Fe_2O_3 states of cluster.[21] The reactivity of $Au_mTi_nO^+_{2n+x}$ cluster ions with CO has been examined for different m, n, and x and supported through mass spectrometry data.[22]

Theoretical studies of the catalytic properties of nanoparticles face several challenges. At first, for sufficiently small nanoparticles (clusters), their properties depend strongly and unpredictably on their size and stoichiometry. Second, even a single cluster will in most cases possess a low symmetry implying that different sites will have different catalytic properties. Third, there may be different paths for the catalytic reaction. Taken together, all these issues make it impossible to obtain a complete description of the catalytic properties of nanoparticles for a given reaction. As an alternative, one may utilize that the catalytic reaction is a local phenomenon that depends mainly on the closest vicinity of the sites at which it takes place. Moreover, by studying some few exemplary cases, one may obtain an understanding on the possible variation in the catalytic properties of the material of interest. In fact, such cluster models have already proven to be very useful to obtain understanding of the catalytic activity at the atomic level. It is this latter approach we shall follow here. Therefore, we emphasize that our results are not expected to provide accurate information on the specific cluster of our study but rather to give general information on the catalytic properties of TiO_2 clusters for the CO oxidation reaction. Accordingly, in the present study we shall consider the $(TiO_2)_6$ cluster to obtain molecular level insights of the catalytic properties of TiO_2 clusters for the CO oxidation. Such models can be treated with accuracy through high level theoretical calculations and hence allow us to peep into structure-reactivity relationships of catalytic materials.[23,24,25]

Despite the abundance of literature on the use of such clusters for CO oxidation, the identification of active sites in the clusters and a molecular-level understanding of this reaction remains elusive. The oxidation of CO may proceed either through the Eley-Rideal (ER) or the Langmuir-Hinshelwood (LH) mechanism. In the ER case, CO or O_2 in the gas phase reacts with the other species that is chemisorbed on the catalyst, so that the role of the catalyst is determined only by its effect on either CO or O_2. In contrast, the LH mechanism involves coadsorption of O_2 and CO on the catalyst and yields an intermediate in which both the molecules are activated.[26] The two mechanisms are competitive depending on the compositions of the catalyst and the activation of the adsorbates on the catalyst. In addition to the above two, there exists another possibility, i.e., the Mars-van Krevelen (MvK) mechanisms where the pre-adsorbed CO molecule directly reacts with the nearest surface lattice oxygen atom to form CO_2.[27] The current study explores all the mechanistic routes for the oxidation of CO by a $(TiO_2)_6$ cluster. In order to obtain a more general insight into the catalytic properties of TiO_2 nanoparticles for this reaction, two different structural isomers of the $(TiO_2)_6$ clusters are considered.

Clusters are often produced in gas phase but will almost always be deposited on some sort of surface for further analysis and applications. The presence of the support can lead to unknown effects on the catalytic properties. Hence, we considered the two isomers of $(TiO_2)_6$ clusters when being deposited on a graphene layer to investigate these effects.

2 | COMPUTATIONAL DETAILS

Initially, a set of candidate structures for $(TiO_2)_n$ clusters were identified using an approach based on genetic algorithms for the unbiased structure optimization and the DFTB-SCC (Density-Functional Tight-Binding Self-Consistent-Charge) method[28] as implemented in the DFTB+ package[29] for the calculation of the total energy for a given structure. Subsequently, the obtained isomers were re-optimized within density-functional theory using the hybrid B3LYP functional[30,31] in conjunction with the 6-31G(d)[32] basis set for both Ti and O atoms as suggested in the literature[33,34].

It has been reported that the clusters with high Vertical Electron Affinity (VEA) are more reactive and can be exploited for applications in catalysis.[35] Therefore, in the present work, the cluster size was selected by analysing global reactivity descriptors like VEA and hardness (η) reported for $(TiO_2)_n$ clusters with $n = 1 \rightarrow 10$.[33] Since η is related to the cluster's resistance to deformation or polarization of its electron cloud, $n = 6$ is selected for the present study because of its minimum hardness and high VEA that favors its reaction with the nucleophilic CO.[33] The reactivity of the clusters is strongly influenced by the geometrical arrangement of atoms. Their catalytic properties can be quantified through reactivity descriptors that can be either global or local descriptors. Among those are the vertical ionization energy (VIE) and VEA that were calculated according to[36]

$$\mathrm{VIE} = E_{\mathtt{cation}} - E_{\mathtt{neutral}} \tag{1}$$

$$\mathrm{VEA} = E_{\mathtt{neutral}} - E_{\mathtt{anion}} \tag{2}$$

Here, $E_{\mathtt{cation}}$, $E_{\mathtt{neutral}}$, and $E_{\mathtt{anion}}$ are the total energies of the cation, the neutral, and the anion cluster at its optimized neutral geometry, respectively. Using the VIE and VEA values, global reactivity descriptors (GRD) like hardness (η), electrophilicity

(χ), chemical potential (μ), and global electrophilicity index (ω) can be evaluated from[37,38,39]

$$\mu = -\frac{1}{2}[\text{VIE} + \text{VEA}] \tag{3}$$

$$\eta = (\text{VIE} - \text{VEA}) \tag{4}$$

$$\omega = \frac{\mu^2}{2\eta} \tag{5}$$

Also the energy gap, E_{gap}, between the highest occupied and lowest unoccupied can be a useful descriptor.

From position-dependent quantities like the charge density and the Fukui functions,atom-decomposed ones can be extracted. This includes the natural bond order (NBO) which we shall discuss in the present work.[40] Moreover, it becomes possible to study the reactivity at the atomic level using the condensed Fukui functions (FF). The condensed forms for atom k in a molecule equals[39,41,33]

$$f_k^+ = q_k(N+1) - q_k(N) \qquad \texttt{for nucleophilic attack} \tag{6}$$

$$f_k^- = q_k(N) - q_k(N-1) \qquad \texttt{for electrophilic attack} \tag{7}$$

where $q_k(N)$, $q_k(N+1)$, and $q_k(N-1)$ are the charges associated with the kth atom in a cluster containing N, $N+1$, and $N-1$ electrons, respectively.

Transition states (TSs) were optimized by using the TS Berny algorithm method.[42] Moreover, vibrational analyses was performed to confirm that intermediates correspond to stable structures and TSs correspond to first order saddle points on the potential energy surface (PES)[43]. Intrinsic reaction coordinate (IRC) calculations[44] established the connectivity of TSs with the local minima. Relative energies of the reactants (R), intermediates (I), TSs, and products (P) were obtained at default temperature and pressure of 298.15 K and 1 atm, respectively.

To include the effects of a support on the catalyst we deposited each of the titanium oxide clusters on a graphene sheet. First, the structures were optimized using the DFTB-SCC method. We treated the graphene as a 2-dimensional periodic system and added the clusters on its surface. A vacuum of about 10 Å was included to assure that there is no interaction between the image systems. The relaxed structures were further optimized at the DFT level using the same functionals and basis set as mentioned above. We considered a finite piece of the graphene layer in the DFT calculations in order to reduce the computational costs. The dangling bonds of the C atoms at the edges of graphene were saturated through hydrogen atoms. Initially, the clusters were deposited on graphene so that their terminal oxygen atoms remain active by pointing away from the graphene surface.

3 | RESULTS AND DISCUSSION

The relative energies and the geometries of various isomers of $(TiO_2)_6$ are shown in Table SI-1 of the supporting information. The isomers chosen for the study of the CO oxidation (S1 and S2) (Fig. 1) are among the more stable ones (see Table SI-1), although, we emphasize, the stability of the isomers is here of only secondary importance as we are focusing on the catalytic properties of structural elements that can be found in TiO_2 nanoparticles.

The S1 isomer has D_{3d} point group symmetry. Each Ti atom is tetrahedrally coordinated with three bridging oxygen atoms (O_b) and one terminal oxygen atom (O_t). The S2 isomer has a distorted symmetry and belongs to C_s point group. It has two Ti atoms (marked as 4 and 11 in Fig. 1) with three bridging and one terminal oxygen atom (O_t) while the remaining four Ti atoms have only bridging oxygen atoms as nearest neighbors.

The reactivity of the clusters species can be quantified in terms of the global and local reactivity descriptors mentioned above. The GRD based descriptors define global reactivity of the cluster as a whole while the LRDs provide estimates of the local selectivity of different sites within the cluster. Since most of these descriptors are obtained as the derivatives of energy and electron density variables, they are reliable parameters in scrutinizing the structure-activity relationship. The values of the GRDs including those of μ, η and ω (obtained using Eqs. 3, 4, and 5) for both S1 and S2 isomers of $(TiO_2)_6$ cluster in gas phase are given in Table 1 . η and μ are key indicators of the overall reactivity of the molecule and the most fundamental descriptors of charge/electron transfer in a chemical reaction. The hardness is related to the cluster's resistance to a deformation or polarization of its electron cloud. The electronic chemical potential can be regarded as the escaping tendency of an electron from a cluster in its ground state. The larger values of η and E_{gap}, and lower values of μ for the S1 isomer in comparison to S2 suggests more stability and lower reactivity (Table 1).

TABLE 1 Global reactivity descriptors (GRDs) of the structural isomers S1 and S2 of Ti_6O_{12} cluster in gas phase. All quantities are given in eV.

Cluster	VIE	VEA	η	μ	ω	E_{gap}
S1	10.98	5.08	5.90	-8.03	3.15	4.35
S2	8.42	4.90	3.52	-6.66	6.30	2.29

In addition to μ and η, the global electrophilicity index (ω), defined by Parr et al.[45] (Eq. 5), measures the energetic stabilization when the system acquires an additional electronic charge from the surrounding. The high ω value for the S2 isomer makes it more susceptible to accept electrons (Table 1).

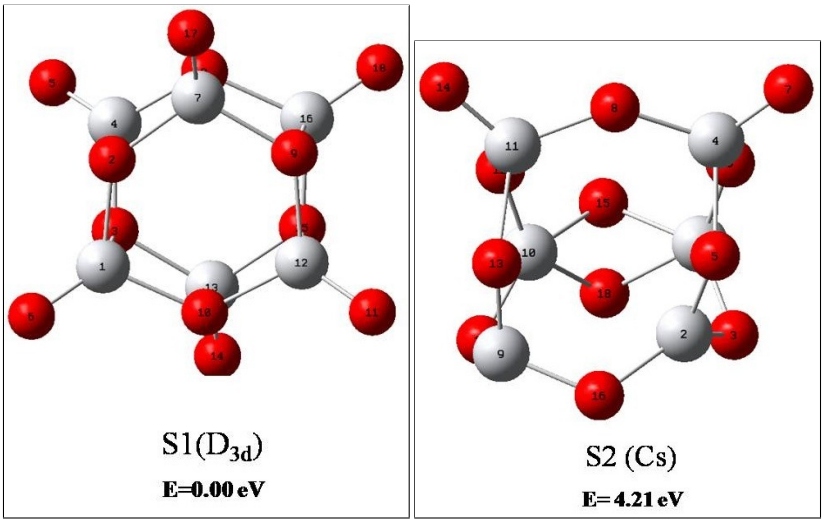

FIGURE 1 Optimized geometries of S1 (left) and S2 isomers (right) of $(TiO_2)_6$ cluster in gas phase. Red spheres represent oxygen and grey spheres represent titanium atoms, respectively.

The global reactivity descriptors cannot distinguish between the reactivities of different sites of a catalyst. On the other hand, since catalysis is mainly a local process a such distinction is important. Therefore, in the present work we shall use local reactivity descriptors as a way of identifying the most reactive sites of different clusters. Thereby, we will identify structural motifs that we expect to occur for clusters of other sizes and/or stoichiometries, also implying that the relative stability of the systems of our study is of secondary importance.

We identified the active sites within a cluster by utilizing LRDs, i.e., first of all the condensed Fukui functions (CFFs). Table 2 contains the CFF values for isomers S1 and S2 of the Ti_6O_{12} cluster in the gas phase. The more negative values of f_k^+ entails more propensity to accept an electron and the corresponding sites are prone to nucleophilic attacks. For the S1 isomer, Ti atoms are the sites susceptible to a nucleophilic attack. The O_t and under-coordinated Ti atoms in the S2 isomer are the sites prone to nucleophilic attacks. In order to check the influence of size on the reactive sites of the cluster, larger clusters $(TiO_2)_{10}$ (shown in Fig. SI-1 of supporting information) were considered. The condensed Fukui function plots shown in Fig. SI-2 confirmed that irrespective of size, terminal oxygens are the reactive sites of the cluster. Therefore, we shall from now on concentrate on the Ti_6O_{12} clusters.

Based on these descriptors, the possible mechanistic routes for CO oxidation using the bare (i.e. without the graphene support) Ti_6O_{12} clusters were investigated in detail considering the different mechanisms mentioned above. Three pathways, labeled as I, II and III, were studied to understand the mechanism of the CO oxidation. In pathways I and II either CO or O_2 is initially adsorbed on the cluster whereas the other reactant remains in the environment until it reacts with the adsorbed species. These two possibilities are examined in pathway I and II, respectively. Here, the role of the catalyst (i.e. cluster) is determined by its binding of CO (in pathway I) or O_2 (in pathway II). For pathway III, we considered co-adsorption of CO and O_2.

TABLE 2 The condensed Fukui functions (f_k^+ and f_k^-) of the atomic sites of S1 and S2 isomers of $(TiO_2)_6$ cluster (depicted in Fig. 1) in gas phases.

Atom Label	Type of atom (S1)	Charge (S1-cluster)	f_k^-	f_k^+	Type of atom (S2)	Charge (S2-cluster)	f_k^-	f_k^+
1	Ti	1.460	-0.016	-0.069	Ti	1.367	-0.126	-0.040
2	O	-0.950	0.010	-0.023	Ti	1.369	-0.133	-0.299
3	O	-0.950	0.056	-0.023	O	-0.813	-0.039	-0.046
4	Ti	1.459	-0.022	-0.069	Ti	1.401	0.004	0.009
5	O	-0.509	0.121	0.121	O	-0.746	-0.044	-0.042
6	O	-0.510	0.102	0.120	O	-0.768	-0.045	-0.047
7	Ti	1.459	-0.017	-0.069	O_t	-0.559	-0.090	-0.092
8	O	-0.950	-0.053	-0.023	O	-0.845	-0.057	-0.013
9	O	-0.950	0.056	-0.023	Ti	1.571	-0.062	-0.299
10	O	-0.950	0.053	-0.023	Ti	1.311	-0.134	-0.040
11	O	-0.509	0.121	0.121	Ti	1.403	0.001	0.017
12	Ti	1.459	-0.022	-0.069	O	-0.758	-0.044	-0.038
13	Ti	1.459	-0.017	-0.069	O	-0.757	-0.029	-0.069
14	O	-0.510	0.104	0.120	O_t	-0.562	-0.086	-0.096
15	O	-0.950	0.010	-0.023	O	-0.449	-0.027	-0.018
16	Ti	1.459	-0.017	-0.069	O	-0.844	-0.030	-0.054
17	O	-0.510	0.104	0.120	O	-0.827	-0.026	-0.048
18	O	-0.510	0.102	0.120	O	-0.495	-0.033	-0.002

Which pathway will be followed depends on the environmental conditions under which the experiment is performed. In particular, it depends on the temperature (T) and chemical potentials of O_2, CO, and CO_2. The thermodynamic stability is determined by the changes in its free energy, ΔG, as compared to pristine cluster and the non-interacting CO and O_2 molecules. The change in the relative free energy (ΔG) at finite temperature and in an environment of CO, O_2, and CO_2 can be written as

$$\Delta G(T) = G_{\text{product}} - G_{\text{cluster}} - \Delta\mu_{\text{gas}}(T). \tag{8}$$

The last term describes the changes when the CO, O_2, or CO_2 molecules leave or enter the environment.[46] In the present study we shall, however, ignore this term.

3.1 | Pathway I: Addition of CO followed by O_2

To follow the pathway I, Ti was chosen as the site (more susceptible to nucleophilic attack with more negative f_k^+) for the reaction for both S1 and S2 isomers. We placed CO near the reacting site and added O_2 to the environment. The pathway I proceeds through these two steps:

- `Step 1: Adsorption of CO on` Ti_6O_{12} `cluster`

$$(TiO_2)_6 + CO \rightarrow (TiO_2)_6 - CO \tag{9}$$

- `Step 2: Reaction of` O_2 `with pre-adsorbed CO`

$$(TiO_2)_6 - CO + O_2 \rightarrow (TiO_2)_6 - O + CO_2. \tag{10}$$

The addition of CO to the S1 isomer leads to the ^{S1}TS1 transition state where the $(TiO_2)_6$-CO complex (^{S1}I1) is formed by passing an energy barrier of 28.63 kcal/mol. The C-O bond is elongated from 1.12 to 1.19 Å. Here, the lone pair of electrons in the CO molecule make it a good nucleophile that binds at the electrophilic site of the cluster (notice, the Ti atoms in S1 have more negative f_k^+ values; see Table 2). Subsequently, the O_2 molecule reacts with ^{S1}I1 (step 2) and forms a stable complex ^{S1}P (Product) by passing through the ^{S1}TS2 state, that has a carbonate group attached to the Ti atom of the S1 cluster. The relative free energy profile is depicted in Fig. 2 .

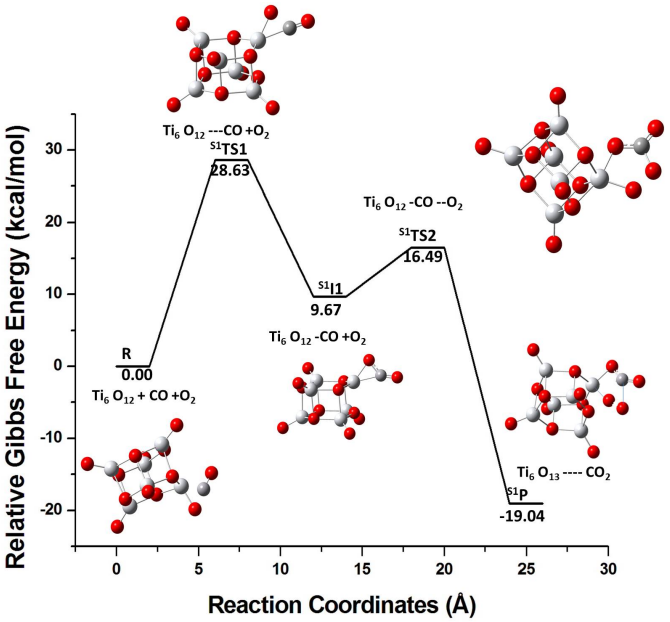

FIGURE 2 The relative free energy profile for the reaction of the S1 isomer with CO followed by a reaction with the O_2 molecule. *R*, ^{S1}TS1, ^{S1}I1, ^{S1}TS2 and ^{S1}P represent reactants, transition state 1, intermediate state 1, transition state 2, and product, respectively.

Fig. 3 shows the energy profile for the same pathway I but for the S2 isomer. The CO molecule binds initially to the O_t atom of the cluster (step 1) via ^{S2}TS1 and ultimately releasing 8.97 kcal/mol. The Ti-O_t bond elongates from 1.60 Å to 2.26 Å. The terminal oxygen atoms in the S2 isomer have high electrophilicity (i.e. have more negative f_k^+ values; cf. Table 2). This explains the strong binding of the nucleophilic CO molecule to O_t in the S2 isomer. In step 2, as O_2 is added to the ^{S2}I1 intermediate state, CO_2 detaches from the cluster and additionally 19.04 kcal/mol energy is released.

Although CO binds to both S1 and S2, the addition of O_2 to the pre-adsorbed CO complex leads to the release of CO_2 only from the S2 isomer. The terminal oxygen atom in the S2 isomer has a strong electrophilic character, and its strong binding with CO facilitates the CO_2 formation via the largely barrier-less TS. This observation is in agreement with the predictions that can be made on the basis of the GRD values. The S2 isomer has higher μ and lower η values that entail its greater reactivity in comparison to the S1 isomer (cf. Table 1). The higher ω value of the S2 isomer suggests that its reaction with CO imparts it higher stability (^{S2}I1 is stabilized by 8.97 kcal/mol in Fig. 3) than that observed for the S1 isomer (^{S1}I1 is 9.67 kcal/mol higher in energy than the pristine cluster in Fig. 2). These observations demonstrate that the geometric arrangement of the atoms in a cluster has strong influence on its reactivity.

The difference in the reactivity of the two forms of Ti_6O_{12} towards CO oxidation through pathway I will be further interpreted by analyzing the frontier orbitals. It is widely accepted that an electron donor (CO in the present case) binds more strongly at that site where the lowest unoccupied molecular orbital (LUMO) protrudes. For the binding to an electron acceptor (O_2 in this case), the highest occupied molecular orbital (HOMO) is involved[47]. For the S1 isomer, CO is pre-adsorbed through a Ti-CO linkage. For S2 the CO molecule binds to an O_t atom. In the S1 form of the Ti_6O_{12} cluster, the LUMO is localized to the Ti atoms (Fig. 4 (a)), but for the S2 isomer, it is concentrated on the O_t atoms (Fig. 4 (b)).

We have further investigated the formation of CO_2 and the carbonate complex in the presence of either the S2 or the S1 isomer by analyzing the HOMO and LUMO of the intermediates (^{S1}I1 and ^{S2}I1) as shown in Fig. 5 . For step 2 of the oxidation, the HOMO is localized to the carbon atom of CO in case of ^{S1}I1 (Fig. 5 (a)). However, for ^{S2}I1 the HOMO is localized to Ti atoms (Fig. 5 (b)). This difference can explain the formation of carbonate in the case of cluster S1 and the release of CO_2 in the case of S2. The reactivity trend as obtained in the present study is well in tune with the conceptual DFT descriptors and reinforces the fact that geometry influences reactivity. Thus, both the GRD and the frontier orbitals help us to rationalize the reactivity of the two structural isomers of the Ti_6O_{12} cluster in the CO oxidation reaction. We are convinced that these results are generally valid, in particular also for other TiO_2 clusters for the CO oxidation reaction.

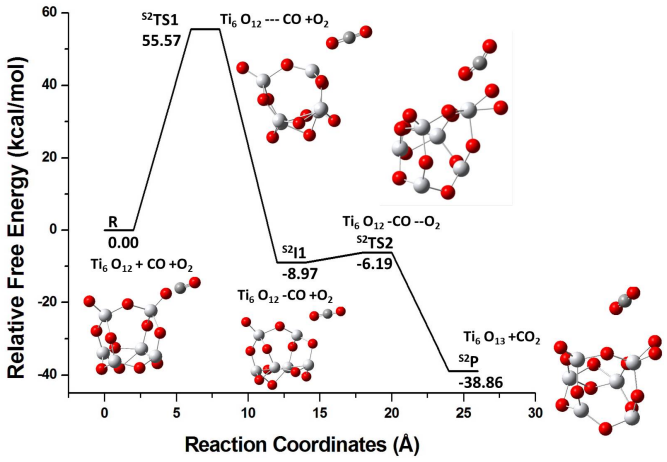

FIGURE 3 The energy profile for the reaction of the S2 isomer through pathway I R, ^{S2}TS1, ^{S2}I1, ^{S2}TS2 and ^{S2}P represent reactants (R), transition state 1 (TS1), intermediate state 1 (I1), transition state 2 (TS2), and product (P), respectively.

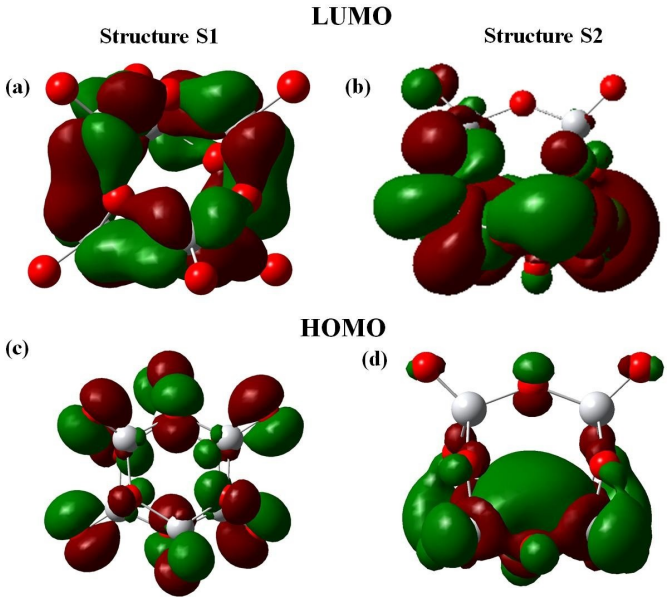

FIGURE 4 The frontier molecular orbitals of the clusters S1 and S2.

3.2 | Pathway II: Addition of O_2 followed by CO

The pathway II explores another possibility of the sequential addition in which the O_2 molecule is pre-adsorbed followed by the reaction with CO,

- `Step 3: Preadsorption of` O_2

$$(TiO_2)_6 + O_2 \rightarrow (TiO_2)_6 - O_2 \tag{11}$$

- `Step 4: Addition of CO`

$$(TiO_2)_6 - O_2 + CO \rightarrow (TiO_2)_6 - O + CO_2 \tag{12}$$

The energy profile for pathway II is shown in Fig. 6 for the S1 isomer. Initially, O_2 is adsorbed on the cluster and the ^{S1}I2 intermediate is formed via ^{S1}TS3. After the addition of CO in step 2, CO_2 and Ti_6O_{13} are produced via ^{S1}TS4 and 25.51 kcal/mol

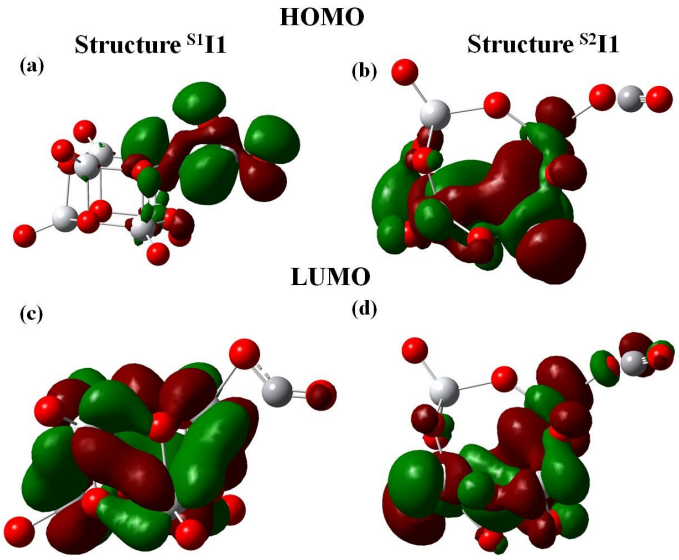

FIGURE 5 The frontier molecular orbitals of the intermediate states obtained in pathway I, ^{S1}I1 and ^{S2}I1.

energy is released. The S2 isomer has a similar route for the pathway II (Fig. 7). In pathway I, the pre-adsorbed CO molecule tends to bind to the electrophilic site of the cluster but the pre-adsorbed O_2 does not bind strongly to the cluster. This can explain the same reactivity of the two isomeric forms in the pathway II since O_2 shows no preference to bind to any cluster site in either form.

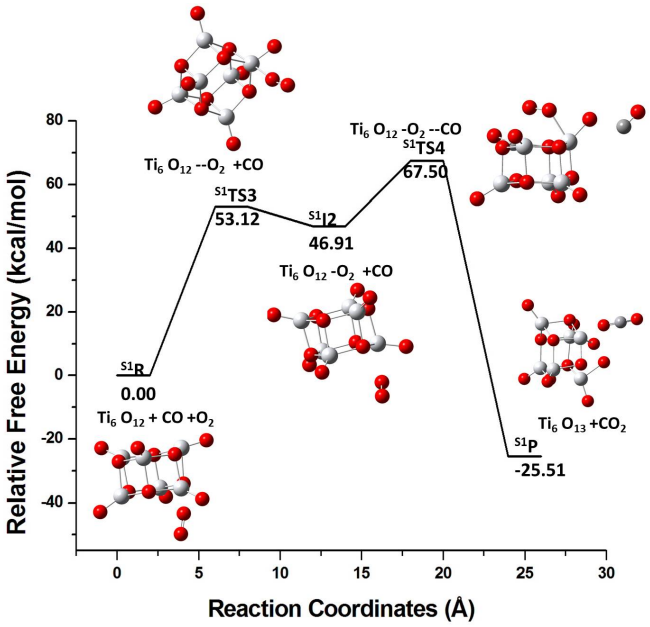

FIGURE 6 Energy profile for the reaction of the S1 isomer with O_2 followed by the reaction with the CO molecule. R, ^{S1}TS3, ^{S1}I2, ^{S1}TS4 and ^{S1}P represents reactants, transition state 3, intermediate state, transition state 4, and product, respectively.

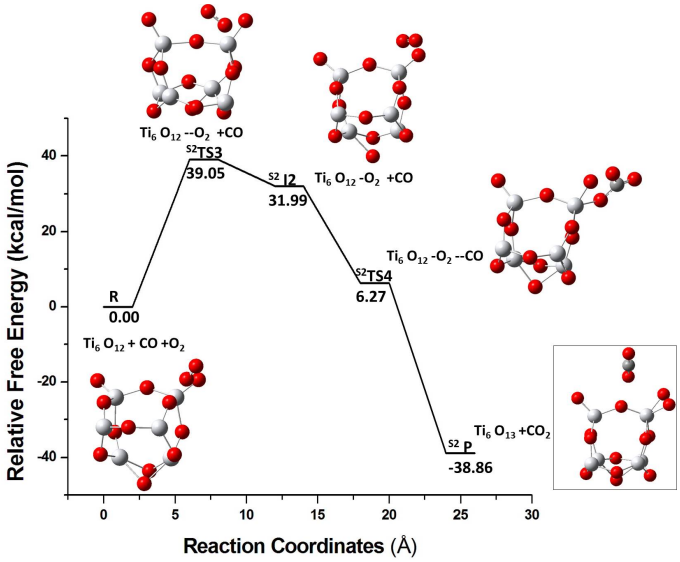

FIGURE 7 The energy profile for the reaction of S2 isomer with O_2 followed by reaction with the CO molecule. R, ^{S2}TS3, ^{S2}I2, ^{S2}TS4 and ^{S2}P represents reactants,transition state 3, intermediate 2,transition state 4, and product, respectively.

3.3 | Pathway III: Co-adsorption of CO and O_2

The energy profile for both the isomers for the CO oxidation via this mechanism is depicted in Fig. 8 . It is based on the initial co-adsorption of CO and O_2. Both S1 and S2 yield CO_2 and Ti_6O_{13} as the products. It is to be noted that the active oxygen which is bonded to CO to form CO_2 is a terminal oxygen of the cluster and not part of the absorbed molecular oxygen. The reaction mechanism observed here is thus analogous to the MvK mechanism in which CO reacts with the oxygen of the catalyst. For the S1 isomer the TS barrier has a value of 67.56 kcal/mol (^{S1}TS5 (Fig. 8 a)). On the contrary, in the case of the S2 isomer, the reaction is essentially barrierless. This may be due to the fact that the S2 isomer has a strong affinity towards CO because of its high reactivity as well as high electron affinity.

For all the three pathways, the molecular oxygen that is absorbed on the cluster is found to play an important role in activating the Ti-O terminal linkage.

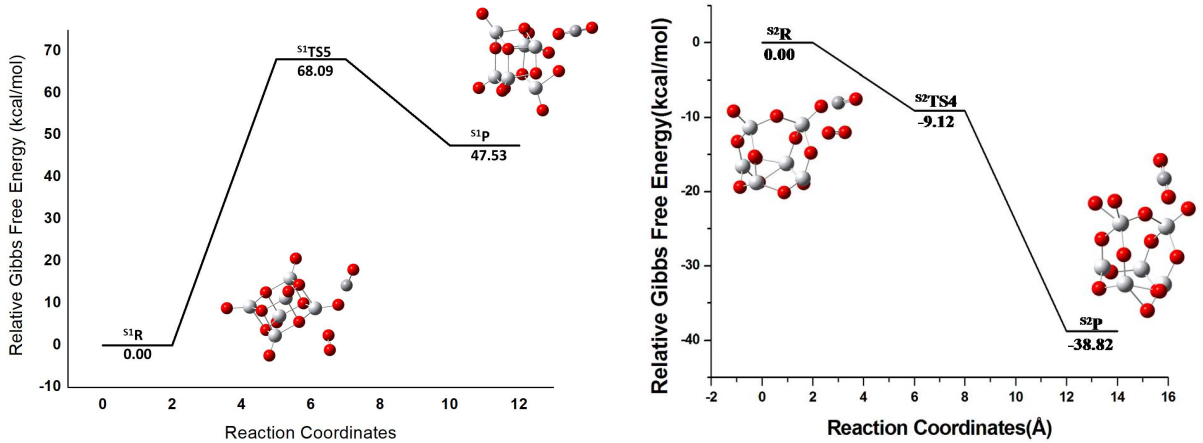

FIGURE 8 Energy profile for the LH mechanism for (upper part) the S1 isomer and (lower part) the S2 isomer. In the upper part, ^{S1}R, ^{S1}TS5 and ^{S1}P represents reactant, transition state 5, and product for the reaction with the S1 isomer as catalyst. In the lower part, ^{S2}R, ^{S2}TS4 and ^{S2}P represents reactant, transition state 4, and product for the reaction with the S2 isomer as catalyst.

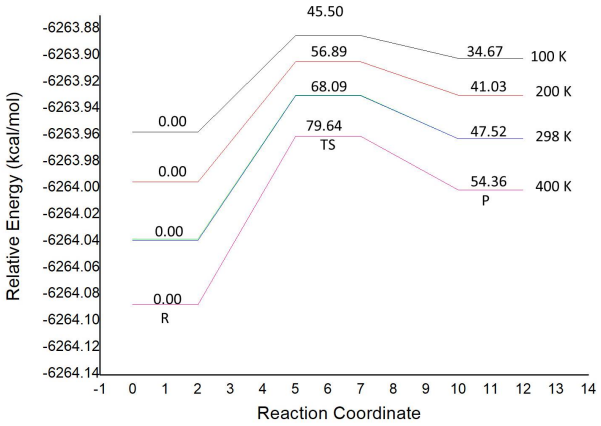

FIGURE 9 Effect of finite temperature on the relative Gibbs free energy for the reaction path 3 for isomer S1 of the $(TiO_2)_6$ cluster.

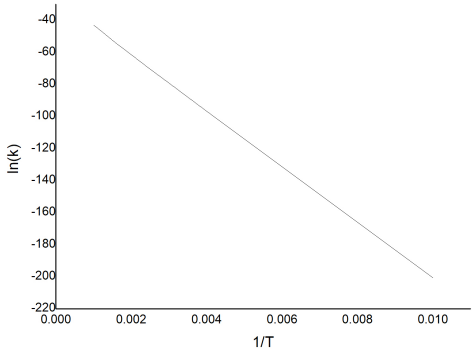

FIGURE 10 Plot of $\ln(k)$ vs $1/T$ for isomer S1 of the $(TiO_2)_6$ cluster.

3.4 | Temperature Dependence

A complete understanding of the effects of temperature on the oxidation of CO in the presence of titanium oxide is crucial for practical applications. We included the effects of temperature within a harmonic approximation and calculated the Gibbs free energies for reactant, transition state, and product. This required the determination of the free energies of the clusters+gas molecules, and of the pristine clusters, as well as the chemical potentials of the gases, i.e. of CO, O_2, and CO_2. We follow a similar approach to that of Bhattacharya et al.[46].

For the reactant, i.e. isomer S1 of $(TiO_2)_6$ cluster in the presence of CO and O_2 gases, we calculate the Gibbs free energy as

$$G_R = F_{\texttt{Cluster}} + \mu_{O_2} + \mu_{CO}, \tag{13}$$

for the transition state as

$$G_T = F_{\texttt{Cluster+gas}}, \tag{14}$$

and for the product as

$$G_P = F_{\texttt{Cluster}} + \mu_{\texttt{CO}_2}. \tag{15}$$

For G_R and G_P, the clusters and gas molecules are non-interacting. The free energies in all cases are calculated as below:

$$F(T) = F^{\texttt{translational}} + F^{\texttt{rotational}} + F^{\texttt{vibrational}} + F^{\texttt{symmetry}} + F^{\texttt{spin}} + F^{\texttt{DFT}} \tag{16}$$

TABLE 3 The condensed Fukui functions (f_k^+ and f_k^-) of the atomic sites of the graphene-supported $(TiO_2)_6$ cluster.

Atom Label	Type of atom (S1)	Charge (S1-cluster)	f_k^-	f_k^+	Type of atom (S2)	Charge (S2-cluster)	f_k^-	f_k^+
1	O	-0.94	-0.041	-0.004	O	-0.86	-0.027	-0.035
2	O	-0.975	-0.011	-0.004	O	-0.724	-0.003	-0.093
3	O	-0.525	-0.079	-0.084	O	-0.771	0.005	-0.028
4	O	-0.541	-0.157	-0.075	O	-0.569	-0.108	-0.061
5	O	-0.962	-0.028	-0.005	O	-0.853	-0.090	-0.012
6	O	0.94	-0.041	-0.004	O	-0.848	-0.114	-0.010
7	O	-0.934	-0.075	-0.005	O	-0.73	0.011	-0.039
8	O	-0.541	-0.156	-0.075	O	-0.582	-0.242	-0.050
9	O	-0.561	-0.108	-0.063	O	-0.576	-0.134	-0.051
10	O	-0.975	-0.010	-0.005	O	-0.877	0.007	-0.016
11	O	-0.538	-0.12	-0.073	O	-0.766	-0.015	-0.036
12	O	-0.524	-0.078	-0.084	O	-0.787	0.001	-0.038
13	Ti	1.472	-0.031	-0.059	Ti	1.611	-0.046	-0.060
14	Ti	1.47	-0.018	-0.080	Ti	1.623	-0.050	-0.453
15	Ti	1.48	-0.022	-0.057	Ti	1.378	-0.039	0.014
16	Ti	1.472	-0.032	-0.058	Ti	1.584	-0.063	-0.039
17	Ti	1.547	-0.022	-0.139	Ti	1.369	-0.043	0.005
18	Ti	1.47	-0.018	-0.081	Ti	1.381	-0.047	-0.001

$$F^{\mathrm{translational}} = -\frac{3}{2}k_B T \ln\left[\frac{2\pi m k_B T}{h^2}\right]$$
$$F^{\mathrm{rotational}} = -k_B T \ln\left[8\pi^2\left(\frac{2\pi k_B T}{h^2}\right)^{3/2}\right] + \frac{1}{2}k_B T \ln(I_A I_B I_C)$$
$$F^{\mathrm{vibrational}} = \sum_i \frac{h\nu_i}{2} + \sum_i k_B T \ln\left[1 - \exp\left(-\frac{h\nu_i}{k_B T}\right)\right]$$
$$F^{\mathrm{symmetry}} = k_B T \ln \sigma$$
$$F^{\mathrm{spin}} = -k_B T \ln \mathcal{M}.$$

In Eq. 16, E^{DFT} is the total energy from a DFT calculation, m is the cluster mass, $I_{A,B,C}$ are the three inertia moments of the cluster, ν_i is the i'th harmonic vibrational frequency, $\mathcal{M}$ is the spin multiplicity, and σ is a symmetry number.

We plot the resulting relative Gibbs free energies for the reaction path 3 (the oxidation of CO in the presence of isomer S1 of $(TiO_2)_6$ cluster) in Fig. 9 for different temperatures T. Raising T clearly increases the reaction barrier. Moreover, the reactants are stabilized compared to the product. This suggests that the oxidation of CO in the presence of S1 isomer of $(TiO_2)_6$ cluster shall be performed at lower T.

Subsequently, we analyze the effect of temperature on the reaction by calculating the reaction rate constants k using the Eyring equation at different T. The plot of $\ln(k)$ vs $1/T$ is shown in Fig. 10 , where a behavior close to linear is observed. Thus, we can assume that the Arrhenius equation is valid here. Then the intercept of $\ln(k)$ axis at $1/T = 0$, i.e., -26.21 s^{-1}, is the value of $\ln(A)$, with A being the pre-exponential factor in the Arrhenius equation. Moreover, the slope of the curve equals then $-E_a/R$ from which we obtain the value for the activation energy, $E_a = 34.77$ kcal/mol.

3.5 | Reactivity of Ti_6O_{12} cluster on graphene support.

Gas-phase models offer computational simplicity for the understanding of the reaction mechanism in detail. However, in experiment the catalyst is often deposited on a surface. Therefore, in the present study, we considered a graphene sheet as a support for the cluster. The 2-D computational model of graphene is a finite $C_{62}H_{20}$ system. The H atoms were used to saturate the dangling bonds of the C atoms at the edges of the finite graphene sheet.

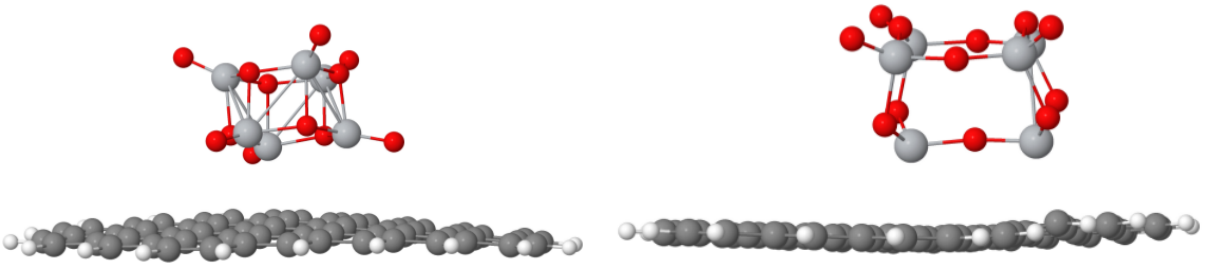

FIGURE 11 The optimized geometries of (left part) S1 and (right part) S2 isomers of Ti_6O_{12} deposited on graphene. Red, grey, and dark grey spheres represent oxygen, titanium, and carbon atoms, respectively.

The optimized structures of the S1 and S2 isomers deposited on the graphene layer are depicted in Fig. 11 . It is seen that no noticeable distortion occurs in the clusters due to the deposition on graphene. We use the adsorption energy of the Ti_6O_{12} isomers (i.e. $E_{\text{adsorption}} = (E_{\text{graphene}} + E_{\text{cluster}}) - E_{\text{graphene-cluster}}$) to quantify the stability of the systems. The adsorption energies are 140.99 kcal/mol for S1 and 112.72 kcal/mol for S2. The high adsorption energy and structural integrity of the cluster in the adsorption process confirms that graphene is suitable as a support for the catalyst. Using the relaxed structure of the two supported clusters we calculated the values of the condensed Fukui functions. The resulting values for S1 and S2 are listed in Table 3 . The values should be compared with those of the gas phase clusters (cf. Tables 2 and 3). Most noteworthy is the case for the S1 isomer for which no positive condensed Fukui function is found after it has been deposited on the graphene sheet. However, overall the absolute values have decreased.

Both the molecular frontier orbitals and the Fukui functions can be used to quantify the changes in the electron density when electrons are added to or removed from the system. Since both properties are used, it is useful to compare these two descriptors. Therefore, we calculated the Fukui functions as functions of position space coordinate (in contrast to the condensed form, where they are separated into atomic components, as reported in Tables 2 and 3).The results are shown in Figs. 12 and 13 for isomers S1 and S2 in gas phase as well as supported on graphene. The green and blue colors correspond to positive and negative regions of the Fukui functions respectively. We recognize immediately that the graphene sheet has a large influence on the reactivity of the cluster and large shifts in the active sites. The right panels in Fig. 12 , for example, show that the graphene has caused one Ti atom to become an active site for nucleophilic reactions, while the other atoms have become less reactive. One can see in the right panels of the figure that a Ti atom has reduced its reactivity in the presence of graphene. On the other hand, in the regions of two O atoms the Fukui function shows values that are more negative.

The influence of the support on the reactivity of the S2 isomer is more complex in comparison to the case of S1. The main effect is a redistribution of the reactive sites. In contrast to the S1 isomer we do not find any single atom that is a highly active site while the others are completely non-reactive.

4 | CONCLUSIONS

In the present work we have investigated the effects of local geometry on the reactivity of TiO_2 clusters for the CO oxidation using Ti_6O_{12} for precise results. We are, however, convinced that our results apply to also other sizes and/or stoichiometries of TiO_2 nanoparticles.

Two structural isomers (S1 and S2) of Ti_6O_{12} clusters were optimized using density functional calculations. The two isomers have contrasting symmetries, with the S1 isomer belonging to the high-symmetric D_{3d} point group while the S2 isomer has a distorted, low C_s symmetry.

Subsequently, their reactivity behavior was investigated whereby we used conceptual density functional descriptors to identify the reactive sites. The ER and LH mechanisms pertaining to sequential and simultaneous adsorption of CO and O_2 on the $(TiO_2)_6$ clusters were studied. We found that the reactivity of the cluster is strongly influenced by its local structure. The analysis of the activation barriers in the free-energy profiles leads us to conclude that the less symmetric S2 isomer is more efficient to catalyze CO oxidation.

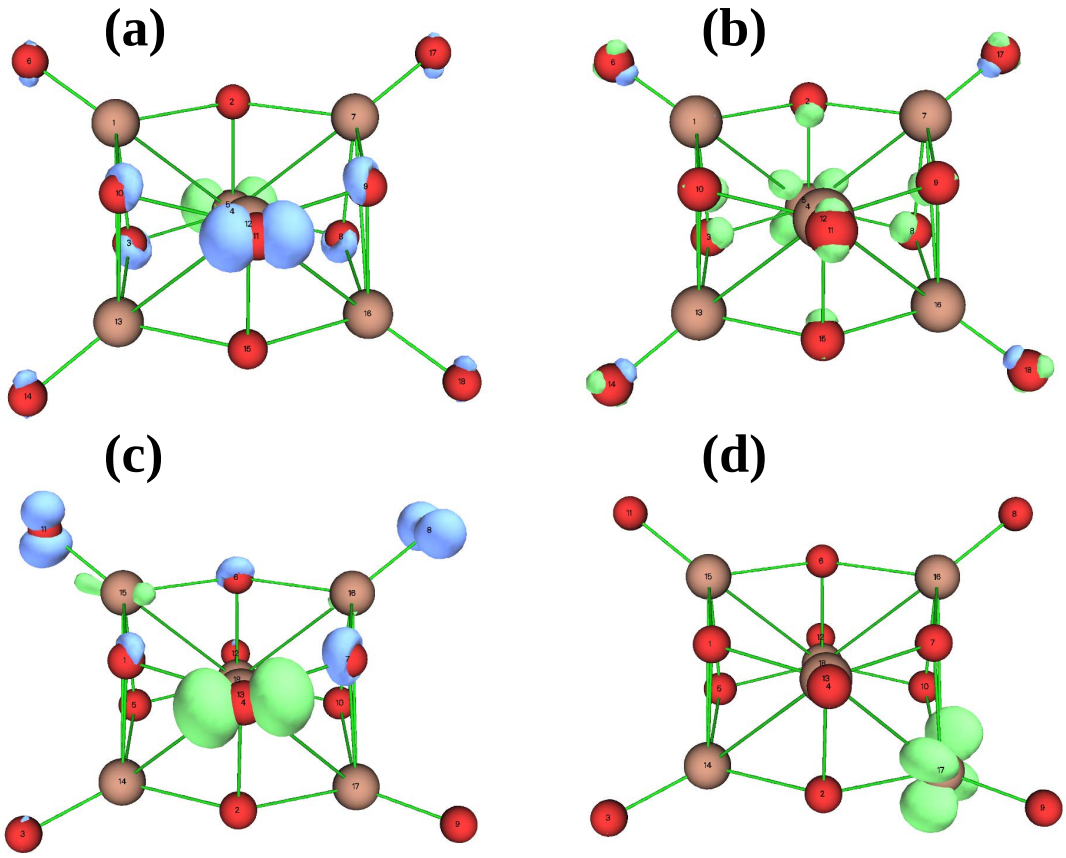

FIGURE 12 Fukui functions of cluster S1 in gas phase (top row) and supported on graphene (bottom row). The left panels show f^- and the right ones f^+.

Most important, maybe, was that we could demonstrate that local and global reactivity descriptors were very helpful in predicting and rationalizing the catalytic activity of the systems of our interest. We believe that this is a general finding, whereby it should become possible to use those in identifying good catalysts.

The effect of raising the temperature on the oxidation of CO in the presence of S1 isomer of $(TiO_2)_6$ cluster was studied through the Gibbs free energies. The reaction barrier was found to become higher as T increases. We calculated the reaction rate constants and using the slope of $\ln(k) - vs - \frac{1}{T}$ found the activation energy $E_a = 34.77$ kcal/mol.

Finally, we studied the effects on the properties of the clusters when these were deposited on a graphene support. Although the structural changes were small, the analysis of the condensed Fukui function suggests that the catalytic properties of the clusters would change.

5 | CONFLICTS OF INTEREST

There are no conflicts to declare.

6 | ACKNOWLEDGEMENT

This project was supported by the German Research Council (DFG) through project SP 439/43-1.

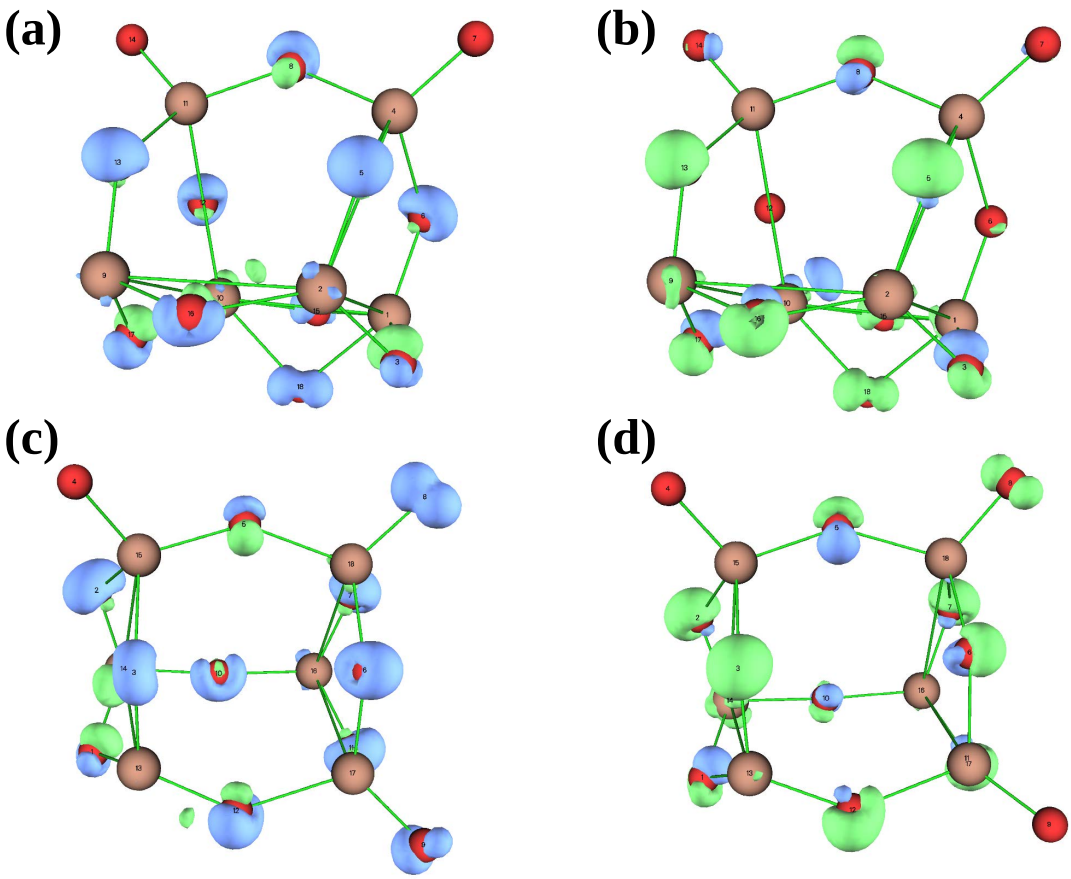

FIGURE 13 Fukui functions of cluster S2 in gas phase (top row) and supported on graphene (bottom row). The left panels show f^- and the right ones f^+.

7 | BIBLIOGRAPHY

References

1. Yumura T, Amenomori T, Kagawa Y, Yoshizawa K. Mechanism for the formaldehyde to formic acid and the formic acid to carbon dioxide conversions mediated by an iron-oxo species. *The Journal of Physical Chemistry A* 2002; 106(4): 621–630.

2. Lin HY, Chen YW, Wang WJ. Preparation of nanosized iron oxide and its application in low temperature CO oxidation. *Journal of Nanoparticle Research* 2005; 7(2-3): 249–263.

3. Li P, Miser DE, Rabiei S, Yadav RT, Hajaligol MR. The removal of carbon monoxide by iron oxide nanoparticles. *Applied Catalysis B: Environmental* 2003; 43(2): 151–162.

4. Wang YZ, Zhao YX, Gao CG, Liu DS. Preparation and catalytic performance of Co 3 O 4 catalysts for low-temperature CO oxidation. *Catalysis Letters* 2007; 116(3-4): 136–142.

5. Lopes I, Davidson A, Thomas C. Calibrated Co3O4 nanoparticles patterned in SBA-15 silicas: Accessibility and activity for CO oxidation. *Catalysis Communications* 2007; 8(12): 2105–2109.

6. Stoyanova M, Konova P, Nikolov P, Naydenov A, Mehandjiev D, others . Alumina-supported nickel oxide for ozone decomposition and catalytic ozonation of CO and VOCs. *Chemical Engineering Journal* 2006; 122(1-2): 41–46.

7. Weng YX, Du LC, Zhang QL, Zhang L. A transient molecular probe for characterizing the surface properties of TiO2 nanoparticle in colloidal solution. *Science and Technology of Advanced Materials* 2005; 6(7): 867.

8. Linsebigler AL, Lu G, Yates Jr JT. Photocatalysis on TiO2 surfaces: principles, mechanisms, and selected results. *Chemical reviews* 1995; 95(3): 735–758.

9. Grätzel M. Photoelectrochemical cells. *nature* 2001; 414(6861): 338.

10. Fujishima A, Honda K. Electrochemical photolysis of water at a semiconductor electrode. *nature* 1972; 238(5358): 37.

11. Buesser B, Grohn A, Pratsinis SE. Sintering rate and mechanism of TiO2 nanoparticles by molecular dynamics. *The Journal of Physical Chemistry C* 2011; 115(22): 11030–11035.

12. Hoffmann MR, Martin ST, Choi W, Bahnemann DW. Environmental applications of semiconductor photocatalysis. *Chemical reviews* 1995; 95(1): 69–96.

13. Thompson TL, Yates JT. Surface science studies of the photoactivation of TiO2 new photochemical processes. *Chemical Reviews* 2006; 106(10): 4428–4453.

14. Hagfeldt A, Boschloo G, Sun L, Kloo L, Pettersson H. Dye-sensitized solar cells. *Chemical reviews* 2010; 110(11): 6595–6663.

15. Widmann D, Behm R. Activation of molecular oxygen and the nature of the active oxygen species for CO oxidation on oxide supported Au catalysts. *Accounts of chemical research* 2014; 47(3): 740–749.

16. Green IX, Tang W, Neurock M, Yates Jr JT. Insights into catalytic oxidation at the Au/TiO2 dual perimeter sites. *Accounts of chemical research* 2013; 47(3): 805–815.

17. Wang YG, Cantu DC, Lee MS, Li J, Glezakou VA, Rousseau R. CO oxidation on Au/TiO2: condition-dependent active sites and mechanistic pathways. *Journal of the American Chemical Society* 2016; 138(33): 10467–10476.

18. Fischer JM, Hankel M, Searles DJ. Computational studies of the interaction of carbon dioxide with graphene-supported titanium dioxide. *The Journal of Physical Chemistry C* 2015; 119(52): 29044–29051.

19. Vajda S, White MG. ACS Catal. 5, 7152 (2015). *ACS Catalysis* 2015; 5: 7152.

20. Tyo EC, Vajda S. Catalysis by clusters with precise numbers of atoms. *Nature nanotechnology* 2015; 10(7): 577.

21. Reddy B, Khanna S. Self-stimulated NO reduction and CO oxidation by iron oxide clusters. *Physical review letters* 2004; 93(6): 068301.

22. Himeno H, Miyajima K, Yasuike T, Mafuné F. Gas Phase Synthesis of Au Clusters Deposited on Titanium Oxide Clusters and Their Reactivity with CO Molecules. *The Journal of Physical Chemistry A* 2011; 115(42): 11479–11485.

23. Nørskov JK, Bligaard T, Logadottir A, et al. Universality in heterogeneous catalysis. *Journal of catalysis* 2002; 209(2): 275–278.

24. Siu CK, Reitmeier S, Balteanu I, Bondybey V, Beyer M. Catalyst poisoning in the conversion of CO and N 2 O to CO 2 and N 2 on Pt 4-in the gas phase. *The European Physical Journal D* 2007; 43(1-3): 189–192.

25. Schrader D, Schwarz H. CH and CC bond activation by bare transition-metal oxide cations in the gas phase. *Angew Chem Int Ed* 1995; 34: 1973–1995.

26. Boreskov GK. *Heterogeneous catalysis*. Nova Publishers . 2003.

27. Doornkamp C, Ponec V. The universal character of the Mars and Van Krevelen mechanism. *Journal of Molecular Catalysis A: Chemical* 2000; 162(1-2): 19–32.

28. Seifert G, Porezag D, Frauenheim T. Calculations of molecules, clusters, and solids with a simplified LCAO-DFT-LDA scheme. *International Journal of Quantum Chemistry* 1996; 58(2): 185-192. doi: 10.1002/(SICI)1097-461X(1996)58:2<185::AID-QUA7>3.0.CO;2-U

29. Aradi B, Hourahine B, Frauenheim T. DFTB+, a Sparse Matrix-Based Implementation of the DFTB Method. *The Journal of Physical Chemistry A* 2007; 111(26): 5678-5684. doi: 10.1021/jp070186p

30. Becke AD. Becke's three parameter hybrid method using the LYP correlation functional. *J. Chem. Phys* 1993; 98: 5648–5652.

31. Lee C, Yang W, Parr R. Density-functional exchange-energy approximation with correct asymptotic behaviour. *Phys. Rev. B* 1988; 37: 785–789.

32. Rassolov VA, Ratner MA, Pople JA, Redfern PC, Curtiss LA. 6-31G* basis set for third-row atoms. *Journal of Computational Chemistry* 2001; 22(9): 976–984.

33. Arab A, Ziari F, Fazli M. Electronic structure and reactivity of (TiO2) n (n= 1–10) nano-clusters: Global and local hardness based DFT study. *Computational Materials Science* 2016; 117: 90–97.

34. Bhattacharya S, Sonin BH, Jumonville CJ, Ghiringhelli LM, Marom N. Computational design of nanoclusters by property-based genetic algorithms: tuning the electronic properties of (TiO 2) n clusters. *Physical Review B* 2015; 91(24): 241115.

35. Marom N, Kim M, Chelikowsky JR. Structure selection based on high vertical electron affinity for TiO 2 clusters. *Physical Review Letters* 2012; 108(10): 106801.

36. Bourcier S, Hoppilliard Y. B3LYP DFT molecular orbital approach, an efficient method to evaluate the thermochemical properties of MALDI matrices. *International Journal of Mass Spectrometry* 2002; 217(1-3): 231–244.

37. Parr RG, Pearson RG. Absolute hardness: companion parameter to absolute electronegativity. *Journal of the American Chemical Society* 1983; 105(26): 7512–7516.

38. Mulliken RS. A new electroaffinity scale; together with data on valence states and on valence ionization potentials and electron affinities. *The Journal of Chemical Physics* 1934; 2(11): 782–793.

39. Yang W, Parr RG. Hardness, softness, and the fukui function in the electronic theory of metals and catalysis. *Proceedings of the National Academy of Sciences* 1985; 82(20): 6723–6726.

40. Glendening ED, Badenhoop JK, Reed AE, et al. NBO 6.0. 2013.

41. Yang W, Mortier WJ. The use of global and local molecular parameters for the analysis of the gas-phase basicity of amines. *Journal of the American Chemical Society* 1986; 108(19): 5708–5711.

42. Schlegel HB. Optimization of equilibrium geometries and transition structures. *Journal of Computational Chemistry* 1982; 3(2): 214–218.

43. Legler C, Brown N, Dunbar R, et al. Scaled quantum mechanical scale factors for vibrational calculations using alternate polarized and augmented basis sets with the B3LYP density functional calculation model. *Spectrochimica Acta Part A: Molecular and Biomolecular Spectroscopy* 2015; 145: 15–24.

44. Fukui K. The path of chemical reactions-the IRC approach. *Accounts of chemical research* 1981; 14(12): 363–368.

45. Parr RG, Szentpály Lv, Liu S. Electrophilicity index. *Journal of the American Chemical Society* 1999; 121(9): 1922–1924.

46. Bhattacharya S, Levchenko SV, Ghiringhelli LM, Scheffler M. Efficient ab initio schemes for finding thermodynamically stable and metastable atomic structures: Benchmark of cascade genetic algorithms. *New Journal of Physics* 2014; 16(12): 123016.

47. Chretien S, Buratto SK, Metiu H. Catalysis by very small Au clusters. *Current Opinion in Solid State and Materials Science* 2007; 11(5-6): 62–75.

How to cite this article: Williams K., B. Hoskins, R. Lee, G. Masato, and T. Woollings (2016), A regime analysis of Atlantic winter jet variability applied to evaluate HadGEM3-GC2, *Q.J.R. Meteorol. Soc.*, *2017;00:1–6*.